Nanoscale

PAPER

View Article Online
View Journal | View Issue

Cite this: *Nanoscale*, 2018, **10**, 7451

Cage-like $Ta@B_n^q$ complexes (n = 23–28, q = −1–+ 3) in 18-electron configurations with the highest coordination number of twenty-eight†

Hai-Ru Li, Hui Liu, Xiao-Qin Lu, Wen-Yan Zan, Xin-Xin Tian, Hai-Gang Lu, Yan-Bo Wu, Yue-Wen Mu * and Si-Dian Li *

Inspired by recent observations of the highest coordination numbers of CN = 10 in planar wheel-type complexes in D_{10h} $Ta@B_{10}^-$ and CN = 20 in double-ring tubular species in D_{10d} $Ta@B_{20}^-$ and theoretical prediction of the smallest endohedral metalloborospherene D_2 $Ta@B_{22}^-$ (**1**) with CN = 22, we present herein the possibility of larger endohedral metalloborospherenes C_2 $Ta@B_{23}$ (**2**), C_2 $Ta@B_{24}^+$ (**3**), C_{2v} $Ta@B_{24}^-$ (**4**), C_1 $Ta@B_{25}$ (**5**), D_{2d} $Ta@B_{26}^+$ (**6**), C_2 $Ta@B_{27}^{2+}$ (**7**), and C_2 $Ta@B_{28}^{3+}$ (**8**) based on extensive first-principles theory investigations. These cage-like $Ta@B_n^q$ complexes with B_6 pentagonal or B_7 hexagonal pyramids on their surface turn out to be the global minima of the systems with CN = 23, 24, 24, 25, 26, 27, and 28, respectively, unveiling the highest coordination number of CN = 28 in spherical environments known in chemistry. Detailed bonding analyses show that **1–8** as superatoms conform to the 18-electron configuration with a universal σ + π double delocalization bonding pattern. They are effectively stabilized *via* spd–π coordination interactions between the Ta center and η^n–B_n ligand which match both geometrically and electronically. Such complexes may serve as embryos of novel metal–boride nanomaterials.

Received 6th February 2018,
Accepted 20th March 2018

DOI: 10.1039/c8nr01087k

rsc.li/nanoscale

1. Introduction

As the fifth element in the periodic table, boron (B[$2s^2 2p^1$]) has a vast variety of molecular structures in chemistry and materials science due to its prototypic electron-deficiency and strong bonding capacity.[1–3] Early density functional theory (DFT) investigations suggest that stable boron clusters and spheres could be constructed from B_6 pentagonal or B_7 hexagonal pyramids (the Aufbau principle).[4] Persistent joint photoelectron spectroscopy (PES) and first-principles theory (FPT) investigations in the past decade on small boron monoanions have established a rich landscape from planar or quasi-planar $B_n^{-/0}$ sheets (n = 3–30, 33–38) to cage-like borospherenes D_{2d} $B_{40}^{-/0}$ and C_3/C_2 B_{39}^- (ref. 2, 3 and 5–10) which may serve as effective inorganic ligands with delocalized multi-center-two-electron ($mc-2e$) σ and π bonds or molecular Wankel motors with an inner wheel rotating in a pseudo-rotating outer bearing.[11,12] Seashell-like $B_{28}^{-/0}$ and B_{29}^- clusters were also observed in PES measurements as minor isomers.[7,8] The borospherene family has been systematically expanded at FPT levels to include the cage-like B_n^q series (n = 36–42, q = n–40) which are composed of twelve interwoven boron double chains (BDCs) with a universal σ + π double delocalization bonding pattern.[13–16] Ion-mobility measurements in combination with DFT calculations, on the other hand, have shown that double-ring tubular B_n^+ monocations (n = 16–25) start to appear at B_{16}^+.[17] Joint PES experimental and FPT theory investigations have further shown that various transition-metal atoms can be coordinated at the centers of monocyclic boron rings or double-ring boron tubes to form perfect wheel-type complexes D_{8h} $Co@B_8^-$, D_{9h} $Ru@B_9^-$, and D_{10h} $Ta@B_{10}^-$ (ref. 18) and drum-like species D_{8d} $Co@B_{16}^-$, D_{9d} $Rh@B_{18}^-$, and D_{10d} $Ta@B_{20}^-$,[19–21] setting the highest possible coordination numbers to CN = 10 in planar environments and CN = 20 in tubular complexes, and pushing the limit of the coordination numbers from the previously reported CN = 15 in $[Th(H_3BNMe_2BH_3)_4]$ and $PbHe_n^{2+}$ and CN = 16 in $MgZn_2$ or $MgNi_2$.[22–25] Based on extensive global minimum searches and FPT calculations, our group recently predicted the possibility of the smallest endohedral metalloborospherenes (EMBs) D_2 $Ta@B_{22}^-$ (**1**) and D_2 $W@B_{22}$ with a higher CN = 22.[26] Detailed orbital and bonding analyses show that these axially chiral transition-metal-centered EMBs follow the 18-electron rule with a σ + π double delocalization bonding pattern.[26] Both theoretical and experimental pieces of evidence indicate that transition-metal dopants lead to earlier planar-

Institute of Molecular Science, Shanxi University, Taiyuan, 034000, China.
E-mail: ywmu@sxu.edu.cn, lisidian@sxu.edu.cn

†Electronic supplementary information (ESI) available. See DOI: 10.1039/c8nr01087k

tubular-spherical structural transitions in boron clusters. However, it still remains unknown to date in both theory and experiments how big such cage-like $M@B_n^q$ complexes may grow in size and what is their highest possible coordination number in spherical environments in chemistry.

Coordination number is an important concept in both chemistry and materials science. The formation of highly coordinated complexes requires the metal center and its ligand to match both geometrically and electronically. The consecutive observations of the biggest planar monocyclic D_{10h} $Ta@B_{10}^-$ with CN = 10 [18] and largest double-ring tubular D_{10d} $Ta@B_{20}^-$ with CN = 20 [21] and theoretical prediction of the smallest EMB D_2 $Ta@B_{22}^-$ with CN = 22 [26] show unique Ta/B compatibility in highly coordinated $Ta@B_n^q$ mononuclear complexes and present the possibility to form bigger EMB $Ta@B_n^q$ complexes with CN > 22. Keeping this inspiration in mind, we aim in this work to locate the largest $Ta@B_n^q$ complexes with the highest coordination number in spherical environments. Interestingly and encouragingly, extensive global minimum searches and FPT calculations indicate that, similar to D_2 $Ta@B_{22}^-$ (**1**),[26] larger Ta-centered EMBs C_2 $Ta@B_{23}$ (**2**), C_2 $Ta@B_{24}^+$ (**3**), C_{2v} $Ta@B_{24}^-$ (**4**), C_1 $Ta@B_{25}$ (**5**), D_{2d} $Ta@B_{26}^+$ (**6**), C_2 $Ta@B_{27}^{2+}$ (**7**), and C_2 $Ta@B_{28}^{3+}$ (**8**) (Fig. 1) with B_6 pentagonal or B_7 hexagonal pyramids on their surface all turn out to be the global minima (GM) of the systems with CN = 23, 24, 24, 25, 26, 27, and 28 in the first coordination shell, respectively, revealing the highest coordination number of CN = 28 in spherical environments known in chemistry. Detailed bonding analyses show that **1–8** as superatoms conform to the 18-electron configuration with a universal σ + π double delocalization bonding pattern and follow the $2(n + 1)^2$ electron counting rule for spherical aromaticity (n = 2). Substituting Ta with its close neighbors result in EMBs $M@B_n^q$ (M = La, Hf, Zr, Nb, and W, n = 22–28) isovalent with **1–8**. The previously predicted $M@B_{40}$ (M = Ca, Sr, Sc, Y, La)[27,28] and observed $M@C_{60}$ (M = Ca, La)[29,30] are excluded from highly coordinated complexes because they are either typical charge-transfer complexes (M = Ca and Sr) or better described as an off-centered metal atom (M = Sc, Y, La) trapped in a fullerene-like cage.[31] The newly proposed singlet $U@B_{40}$ [32] appears to have a wavefunction instability leading to an open-shell off-centered structure.

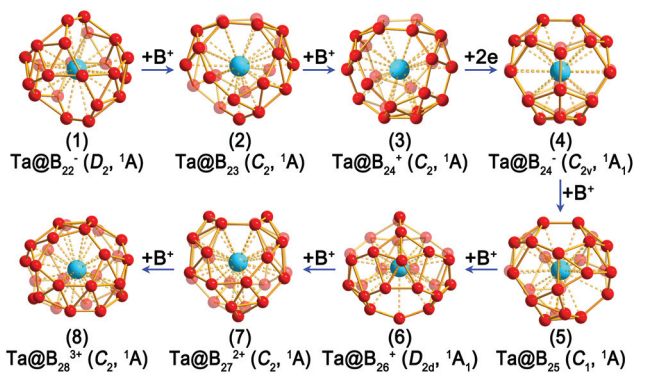

Fig. 1 Optimized endohedral metalloborospherenes D_2 $Ta@B_{22}^-$ (**1**), C_2 $Ta@B_{23}$ (**2**), C_2 $Ta@B_{24}^+$ (**3**), C_{2v} $Ta@B_{24}^-$ (**4**), C_1 $Ta@B_{25}$ (**5**), D_{2d} $Ta@B_{26}^+$ (**6**), C_2 $Ta@B_{27}^{2+}$ (**7**), and C_2 $Ta@B_{28}^{3+}$ (**8**) at the PBE0 level.

2. Computational methods

Extensive GM searches for neutral or charged TaB_n clusters (n = 23–29) were performed using both the Minima Hopping algorithm[33,34] and TGmin code based on the Basin-Hopping method[35,36] at the DFT level, in combination with manual structural constructions from known $B_n^{-/0/+}$ clusters.[2,3,5–10] Over 5000 stationary points are explored for each system at the PBE/DZVP level[37] using the CP2K program.[38] The low-lying isomers were then fully optimized at the PBE0[39] level with the 6-311+G* basis set[40] for B and Stuttgart relativistic small-core pseudopotential and valence basis sets for Ta, La, Hf, Zr, Nb, and W[41,42] using the Gaussian 09 program.[43] Single-point energies of the ten lowest-lying isomers were further refined at the PBE0 geometries using the CCSD(T) method[44–46] implemented in MOLPRO.[47] Chemical bonding analyses were performed using the adaptive natural density partitioning (AdNDP) approach at the PBE0 level.[48] Natural bonding analyses were performed using the NBO 6.0 program.[49] Molecular dynamics (MD) simulations were done on $Ta@B_{24}^-$ (**4**) for 30 ps at different temperatures using the CP2K code.

3. Results and discussion

All the GMs thus obtained (**2–8**) (Fig. 1) and most of the low-lying isomers in the configuration energy spectra of the concerned species at the CCSD(T) level (Fig. 2 and Fig. S1†) turn

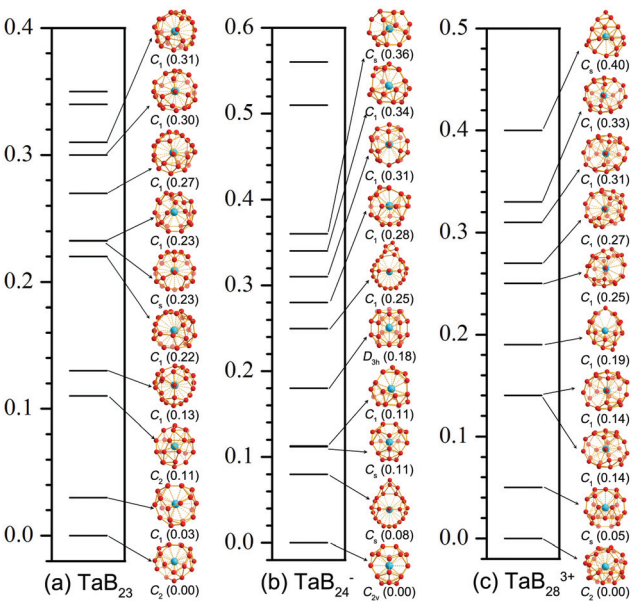

Fig. 2 Configurational energy spectra of (a) TaB_{23}, (b) TaB_{24}^-, and (c) TaB_{28}^{3+} with relative energies indicated in eV at the CCSD(T) level.

out to have cage-like geometries with B_6 pentagonal or B_7 hexagonal pyramids and polygonal holes on their surface, in line with the Aufbau principle.[4] We briefly discuss the most important isomers in the following sections starting from the axially chiral C_2 Ta@B_{23} (**2**) which possesses two B_6 pentagonal pyramids on two shoulders, two heptagons in front and back, and two octagons at two sides. It features two equivalent B_9 BDCs spiraling up on the waist around the C_2 molecular axis, similar to D_2 Ta@B_{22}^- (**1**).[26] The second lowest-lying C_1 Ta@B_{23} with two B_6 pentagonal pyramids on two shoulders lies only slightly higher than the GM (by 0.03 eV) (Fig. 2a).

The addition of one B^+ into Ta@B_{23} produces the axially chiral C_2 Ta@B_{24}^+ (**3**) with CN = 24 which possesses two B_6 pentagonal pyramids on two shoulders, two heptagons in front and back, two hexagons on the waist, and two edge-sharing B_6 pentagonal pyramids at the bottom. The second isomer C_1 Ta@B_{24}^+ with a B_7 unit atop a distorted double-ring tubular Ta@B_{17} lies 0.10 eV above the GM (Fig. S1†). The third high-symmetry isomer D_{2d} Ta@B_{24}^+ with a relative energy of 0.23 eV has a perfect tetragonal geometry with four equivalent B_6 pentagonal pyramids at four corners.

The attachment of two extra electrons to Ta@B_{24}^+ generates the high-symmetry C_{2v} Ta@B_{24}^- (**4**) with CN = 24 which can be conveniently constructed from the smallest fullerene C_{20}[50] by capping two singly interconnected pentagons on the top and two edge-sharing pentagons at the bottom, with four B_6 pentagonal pyramids and eight pentagons formed on the surface. The second isomer C_s Ta@B_{24}^- with a B_3 bridge atop an elongated double-ring tubular Ta@B_{21} lies 0.08 eV higher than the GM (Fig. 2b). The third structure C_s Ta@B_{24}^- which is a positional isomer of Ta@B_{24}^- (**4**) with a relative energy of 0.11 eV turns out to be iso-energetic with the fourth low-symmetry C_1 Ta@B_{24}^-. The fifth high-symmetry isomer D_{3h} Ta@B_{24}^- which has the same geometry as the previously predicted isovalent D_{3h} W@B_{24}[51] lies 0.18 eV higher than the C_{2v} GM. We obtain two new positional isomers C_{2v} W@B_{24} and C_s W@B_{24} for neutral WB_{24} shown in Fig. S2† which appear to be 0.26 eV and 0.08 eV more stable than the previously reported D_{3h} W@B_{24}[51] at CCSD(T), respectively, with C_{2v} W@B_{24} being overwhelmingly the GM of the system. Extensive MD simulations (Fig. S3†) indicate that Ta@B_{24}^- (**4**) remains dynamically stable at 400 K with the small root-mean-square-deviation of RMSD = 0.07 Å and the maximum bond length deviation of MAXD = 0.21 Å. It starts to hop between C_{2v} GM and its positional isomer C_s Ta@B_{24}^- at 450 K in a concerted mechanism mainly involving one tetracoordinate B atom.

The addition of another B^+ into Ta@B_{24}^- results in the low-symmetry C_1 Ta@B_{25} (**5**) with CN = 25 which contains one B_6 pentagonal pyramid on one shoulder and one B_7 hexagonal pyramid on the other (Fig. S1†). With one more B^+, the high-symmetry D_{2d} Ta@B_{26}^+ (**6**) with CN = 26 is achieved, which possesses four equivalent B_6 pentagonal pyramids on the waist and two $-B^-$ bridges on the top and bottom. Adding one more B^+ into the system produces the axially chiral C_2 Ta@B_{27}^{2+} (**7**) with CN = 27 which possesses two pairs of interconnected pentagonal pyramids on two shoulders and five hexagons on the surface. Replacing Ta in **2**–**7** with Hf generates their isovalent counterparts C_2 Hf@B_{23}^-, C_2 Hf@B_{24}, C_{2v} Hf@B_{24}^{2-}, C_1 Hf@B_{25}^-, D_{2d} Hf@B_{26}, and C_2 Hf@B_{27}^+, respectively, which are all true minima of the systems possible to be observed in experiments.

The highest coordination number of CN = 28 in the EMB family is achieved in the axially chiral C_2 Ta@B_{28}^{3+} (**8**) which features three interwoven BDCs on the surface, with two equivalent B_6 pentagonal pyramids formed on two sides. The seashell-like C_2 Ta@B_{28}^{3+} obtained from the observed C_2 B_{28}^- (ref. 7) turns out to be much less stable than the C_2 GM (by 0.76 eV). With Ta–B distances between r_{Ta-B} = 2.50 and 2.92, Ta–B Wiberg bond indexes between WBI_{Ta-B} = 0.16 and 0.28, and total Ta bond index of WBI_{Ta} = 6.09 (Table S1†), all the 28 B atoms in Ta@B_{28}^{3+} (**8**) can be viewed as effective ligands to the Ta center. Substituting Ta in Ta@B_{28}^{3+} (**8**) with La, Hf, Zr, and Nb produces its isovalent counterparts C_2 La@B_{28}^+, C_2 Hf@B_{28}^{2+}, C_2 Zr@B_{28}^{2+}, and C_2 Nb@B_{28}^{3+} which are all true minima of the systems.

However, with one more B^+ added in, TaB_{29}^{4+} appears to favor an elongated C_1 Ta@B_{29}^{4+} which contains two B atoms squeezed out of the first coordination shell with r_{Ta-B} > 3.00 Å (Fig. S4†). The second isomer C_1 Ta@B_{29}^{4+} with a relative energy of 0.10 eV also possesses one B atom with r_{Ta-B} > 3.00 Å. The much concerned seashell-like C_2 Ta@B_{29}^{4+} originating from the observed C_2 B_{29}^- (ref. 8) turns out to be 0.96 eV less stable than the GM. Ta@B_{29}^{4+} thus has an effective coordination number of CN = 29–2 = 27 with the total Ta bond index of WBI_{Ta} = 6.10 which is slightly lower than the corresponding value of 6.22 in C_2 Ta@B_{27}^{2+} (**7**). In the previously reported $PbHe_n^{2+}$ clusters (n = 2–15), Pb–He coordination bond lengths in the first coordination shell have been predicted to be between r_{Pb-He} = 2.595 and 2.869 Å < 3.0 Å,[23] supporting the proposed coordination bond length criterion of 3.0 Å for the Ta@B_n^q series concerned in this work. Ta@B_n^q with $q \geq +4$ are not expected to exist in experiments due to Coulomb explosions. We conclude that the isovalent C_2 La@B_{28}^+, C_2 Hf@B_{28}^{2+}, and C_2 Ta@B_{28}^{3+} (**8**) have achieved the highest coordination number of CN = 28 in spherical environments known in chemistry. Ta and its close neighbors La, Hf, Zr, Nb, and W with the largest atomic radii in transition metals and partially filled electronic configurations of M[$(n-1)d^{1-4}ns^2$] exhibit strong propensity to form highly coordinated complexes with suitable ligands. Boron, the first electron-deficient nonmetal element in the periodic table with a small atomic radius and partially filled 2p atomic orbitals which form effective p → d back donations from B_n ligands to metal centers, generates optimum wheel-type planar, double-ring tubular, and cage-like η^n–B_n ligands with high coordination numbers to match transition metals like Ta both geometrically and electronically.[18,21,26] As indicated in Fig. S5,† the coordination numbers of M@B_n^q complexes increase linearly and continuously in the size range between n = 8 and 28 and reach the maximum value of CN = 28 at Ta@B_{28}^{3+} (**8**) and La@B_{28}^+, with a planar region (n = 8–10) including D_{8h} Co@B_8^-, D_{9h} Ru@B_9^-, and D_{10h} Ta@B_{10}^-,[18] a tubular area

(n = 16–22) covering D_{8d} Co@B_{16}^-, D_{9d} Rh@B_{18}^-, D_{10d} Ta@B_{20}^-, C_s Ta@B_{20}^-, D_{10d} Ta@B_{20}^-,[19–21] C_s Ta@B_{21}, and C_{3v} Ta@B_{22}^+,[24] and a spherical domain (n = 22–28) including **1–8**. The CN value abruptly drops to CN = 27 at Ta@B_{29}^{4+} and La@B_{29}^{2+} with n = 29. Cage-like B_n ligands with more than 28 atoms appear to have too big cavities to coordinate a transition metal stably at the center, as evidenced by the off-centered metal atoms in M@B_{40} (M = Sc, Y, La) and La@C_{60}.[28,30]

The high stabilities of **1–8** originate from their unique electronic configurations and bonding patterns. We choose the high-symmetry C_{2v} Ta@B_{24}^- (**4**) as an example to analyze its canonical molecular orbitals (CMOs) and AdNDP bonding patterns in detail. It has the shortest average Ta–B distance of R_{av} = 2.47 Å and the highest total Ta bond index of WBI_{Ta} = 6.33 in the EMB family (Table S1†). Fig. 3a compares the eigenvalue spectra of the bare cage-like C_{2v} B_{24} ligand and the C_{2v} Ta@B_{24}^- (**4**) complex, with nine π CMOs perpendicular to the cage surface depicted. The C_{2v} B_{24} ligand has six occupied π-orbitals HOMO(b_2), HOMO−1(b_1), HOMO−7(b_2), HOMO−11 (b_1), HOMO−12(a_1), and HOMO−15(a_1) and three unoccupied π-orbitals LUMO(a_1), LUMO+1(a_1), and LUMO+2(a_2), with a narrow HOMO–LUMO energy gap of ΔE_{gap} = 1.10 eV. These out-of-surface π-orbitals originating from the partially filled B $2p_z$ atomic orbitals interact effectively with the partially filled valence-shell orbitals of the Ta center [$5d^36s^2$] to form nine hybridized molecular orbitals in Ta@B_{24}^- (**4**), *i.e.*, HOMO−5 (d_{xz}), HOMO−6(d_{xy}), HOMO−7($d_{x_2-y_2}$), HOMO−8(d_{z_2}), HOMO−9(d_{yz}), HOMO−13(p_x), HOMO−16(p_y), HOMO−17(p_z), and HOMO−21(s), with a much larger HOMO–LUMO gap of ΔE_{gap} = 3.86 eV. Such a superatomic electronic configuration follows the 18-electron rule in stable transition-metal complexes (such as in the 18-electron ferrocene $Fe(C_5H_5)_2$ and bis(benzene)chromium $Cr(C_6H_6)_2$), *i.e.* $n_{ligand} + n_{metal} - q = 18$, where n_{ligand} = 12 stands for the number of π electrons of the cage-like B_{24} ligand, n_{metal} = 5 the number of valence electrons of the metal center Ta, and q = −1 the charge state of the complex. Such spd–π coordination interactions can be clearly visualized in the electron density difference map of Ta@B_{24}^- (**4**) shown in Fig. 3b which reveals obvious electron accumulation in regions between the Ta center and cage-like B_{24} ligand. As shown in Fig. S6,† similar to **1** and **4**, **2**, **3**, **5–8** each have nine occupied atomic-like π-CMOs with large HOMO–LUMO gaps between 3.39 and 4.08 eV. Thus, **1–8** as superatoms all follow the 18-electron rule to form stable complexes. As specific examples, C_2 Ta@B_{24}^+ (**3**) and C_{2v} Ta@B_{24}^- (**4**) in different charge states possess different B_{24} ligand structures to match the 18-electron configuration with n_{ligand} = 14 and 12, respectively.

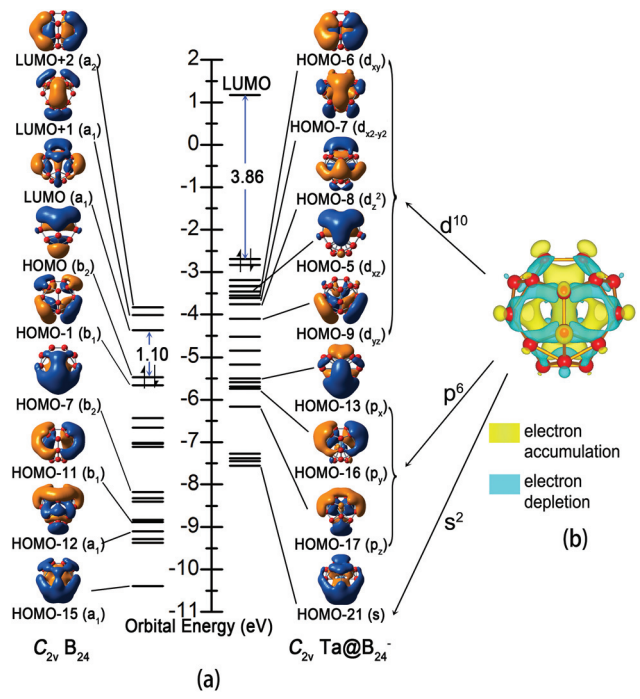

Fig. 3 Comparison of the eigenvalue spectra of the bare cage-like C_{2v} B_{24} ligand and the C_{2v} Ta@B_{24}^- (**4**) complex with the HOMO–LUMO energy gaps indicated in eV at the PBE0 level. (b) Electron density difference map of Ta@B_{24}^- (**4**), with regions of increased and decreased electron densities indicated in yellow and blue, respectively.

Natural bonding orbital (NBO) analyses show that the Ta center in Ta@B_{24}^- (**4**) possesses the electronic configuration of $5d^{4.91}6s^{0.43}$ and the negative natural charge of −0.64|*e*|, showing that Ta donates most of its $5s^2$ electrons to the spherical B_{24} ligand, while its partially occupied 5d orbital, in return, accepts approximately two electrons (~1.91|*e*|) from the out-of-surface p_π orbitals of the cage-like η^{24}–B_{24} ligand *via* effective $p_\pi \rightarrow d$ back donations. The average Ta–B distance of r_{av} = 2.47 Å in Ta@B_{24}^- (**4**) is the same as the corresponding value of r = 2.47 Å in D_{10h} Ta@B_{10}^- and shorter than that of 2.67 Å in D_{10d} Ta@B_{20}^-.[18–21] Its average Ta–B bond order of WBI_{Ta-B} = 0.26 also appears to be well comparable to the Ta–B bond order of WBI_{Ta-B} = 0.24 in D_{10d} Ta@B_{20}^- (ref. 21) and the Fe–C bond order of WBI_{Fe-C} = 0.30 in D_{5h} $Fe(C_5H_5)_2$. In fact, **1–8** have higher total Ta bond orders of WBI_{Ta} = 5.91–6.33 (Table S1†) than the corresponding values of 5.87, 5.74, 5.69, 4.19, and 3.06 calculated for the metal centers in tubular C_{3v} B_4–Ta@B_{18}^+, C_s B_3–Ta@B_{18},[26] C_s B_2–Ta@B_{18}^-,[21] and sandwich-like D_{6h} $Cr(C_6H_6)_2$ and D_{5h} $Fe(C_5H_5)_2$, respectively. NBO calculations further indicate that all the Ta centers in **2–8** carry negative atomic charges with q_{Ta} = −0.14 to −0.64|*e*| (Table S1†), showing strong $p_\pi \rightarrow d$ back-donation from the B_n ligand to the Ta center in these complexes (especially in cationic complexes **3**, **6**, **7**, and **8**). The calculated average r_{av} = 2.47–2.68 Å and WBI_{Ta-B} = 0.22–0.27 in **1–8** also well support the formation of spherical coordination interactions in the EMB family.

AdNDP bonding analyses recover both localized and delocalized bonding interactions of the systems. As shown in Fig. S7c,† Ta@B_{24}^- (**4**) possesses 11 2c–2e B–B σ bonds connecting the four B_6 pentagonal pyramids, 18 3c–2e σ bonds on 18 B_3 triangles, and 1 4c–2e σ bond on the B_4 rhombus between the two edge-sharing pentagonal pyramids at the bottom. There exist nine delocalized π bonds over the σ-skeleton involving the Ta center which correspond to the nine

delocalized π CMOs depicted in Fig. 3, *i.e.*, 2 5c–2e π bonds over two tricoordinate >B$^-$ sites in the front and back, 2 6c–2e π bonds over two pentagons on two sides, 1 7c–2e π bond on the top, 2 7c–2e π bonds over two doubly interconnected pentagonal pyramids on two shoulders, and 2 7c–2e π bonds over the two edge-sharing pentagonal pyramids at the bottom. Ta@B_{24}^- (**4**) thus possesses a σ + π double delocalization bonding pattern and conforms to the $2(n + 1)^2$ electron counting rule for spherical aromaticity (n = 2). As shown in Fig. S7,† endohedral complexes **1–8** in 18-electron configurations follow the universal bonding pattern of σ + π double delocalization, similar to bare B_n^q borospherenes (n = 36–42, $q = n$–40).[5,6,13–16]

The infrared (IR), Raman, and UV-vis spectra of Ta@B_{24}^- (**4**) are computationally simulated and are shown in Fig. 4 to facilitate their future experimental characterization studies. Infrared photodissociation has proven to be a powerful means to characterize novel clusters in gas phases.[52] Ta@B_{24}^- (**4**) features five major IR active peaks around 285.3(b_1), 369.8(a_1), 425.5(b_2), 683.1(b_2), and 705.3(b_1) cm^{-1} and two major Raman scattering peaks around 606.1(a_1) and 643.2(a_1) cm^{-1}, respectively. The strongest Raman peak at 643.2(a_1) corresponds to the typical symmetrical radial breathing mode of the endohedral cage-like complex which can be used to characterize hollow structures.[53] The strong UV bands around 222, 263, 283, and 301 nm mainly originate from electronic transitions from deep inner shells of the monoanion to its high-lying unoccupied molecular orbitals, while the weak bands above 400 nm involve electronic excitation from the HOMO and HOMO−1. IR, Raman, and UV-vis spectra have also been simulated for **2**, **3**, and **5–8** in Fig. S8.†

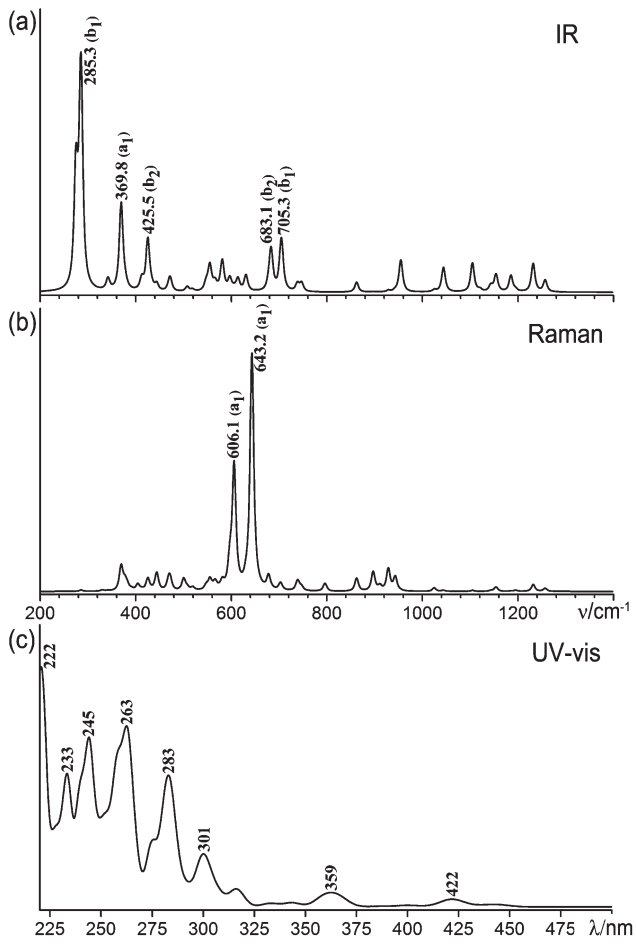

Fig. 4 Simulated (a) IR, (b) Raman, and (c) UV-vis spectra of Ta@B_{24}^- (**4**) at the PBE0 level.

4. Conclusion

In summary, we have presented the possibility of the 18-electron Ta@B_n^q family including Ta@B_{22}^- (**1**), Ta@B_{23} (**2**), Ta@B_{24}^+ (**3**), Ta@B_{24}^- (**4**), Ta@B_{25} (**5**), Ta@B_{26}^+ (**6**), Ta@B_{27}^{2+} (**7**), and Ta@B_{28}^{3+} (**8**), uncovering the highest coordination number of CN = 28 in spherical complexes known in chemistry. These cage-like complexes with B_6 pentagonal or B_7 hexagonal pyramids on their surface in delocalization bonding patterns possess much higher coordination numbers than the previously predicted $PbHe_n^{2+}$ in a hard-sphere model with weak He–He van der Waals interactions.[22] Borospherene ligands with triangular units on their cage surface also provide higher coordination numbers than the corresponding carbon fullerenes which are composed of only hexagons and pentagons. The unique Ta/B compatibility facilitates the formation of a complete set of Ta@B_n^q complexes with the highest CN = 10, 20, and 28 in planar, tubular, and spherical environments, respectively. Such complexes which are possible to be synthesized *via* co-vaporization of boron and desired transition metals may serve as embryos of novel metal–boride nanomaterials.

Conflicts of interest

There are no conflicts to declare.

Acknowledgements

The work was supported by the National Natural Science Foundation of China (21720102006 to S.-D. Li, 11504213 to Y.-W. Mu, 21473106 to H.-G. Lu, U1510103 to X.-X. Tian).

Notes and references

1 W. N. Lipscomb, *Science*, 1977, **196**, 1047.
2 L. S. Wang, *Int. Rev. Phys. Chem.*, 2016, **35**, 69.
3 A. P. Sergeeva, I. A. Popva, Z. A. Piazza, W. L. Li, C. Romanescu, L. S. Wang and A. I. Boldyrev, *Acc. Chem. Res.*, 2014, **47**, 1349.
4 I. Boustani, *Phys. Rev. B: Condens. Matter Mater. Phys.*, 1997, **55**, 16426.
5 H. J. Zhai, Y. F. Zhao, W. L. Li, Q. Chen, H. Bai, H. S. Hu, Z. A. Piazza, W. J. Tian, H. G. Lu, Y. B. Wu, Y. W. Mu,

G. F. Wei, Z. P. Liu, J. Li, S. D. Li and L. S. Wang, *Nat. Chem.*, 2014, **6**, 727.
6 Q. Chen, W. L. Li, Y. F. Zhao, S. Y. Zhang, H. S. Hu, H. Bai, H. R. Li, W. J. Tian, H. G. Lu, H. J. Zhai, S. D. Li, J. Li and L. S. Wang, *ACS Nano*, 2015, **9**, 754.
7 Y. J. Wang, Y. F. Zhao, W. L. Li, T. Jian, Q. Chen, X. R. You, T. Ou, X. Y. Zhao, H. J. Zhai, S. D. Li, J. Li and L. S. Wang, *J. Chem. Phys.*, 2016, **144**, 064307.
8 H. R. Li, T. Jian, W. L. Li, C. Q. Miao, Y. J. Wang, Q. Chen, X. M. Luo, K. Wang, H. J. Zhai, S. D. Li and L. S. Wang, *Phys. Chem. Chem. Phys.*, 2016, **18**, 29147.
9 Q. Chen, W. J. Tian, L. Y. Feng, H. G. Lu, Y. W. Mu, H. J. Zhai, S. D. Li and L. S. Wang, *Nanoscale*, 2017, **9**, 4550.
10 Q. Chen, W. L. Li, X. Y. Zhao, H. R. Li, L. Y. Feng, H. J. Zhai, S. D. Li and L. S. Wang, *Eur. J. Inorg. Chem.*, 2017, 4546–4551.
11 Y. J. Wang, X. Y. Zhao, Q. Chen, H. J. Zhai and S. D. Li, *Nanoscale*, 2015, **7**, 16054.
12 Y. Yang, D. Jia, Y. J. Wang, H. J. Zhai, Y. Man and S. D. Li, *Nanoscale*, 2017, **9**, 1443.
13 Q. Chen, S. Y. Zhang, H. Bai, W. J. Tian, T. Gao, H. R. Li, C. Q. Miao, Y. W. Mu, H. G. Lu, H. J. Zhai and S. D. Li, *Angew. Chem., Int. Ed.*, 2015, **54**, 8160.
14 Q. Chen, H. R. Li, C. Q. Miao, Y. J. Wang, H. G. Lu, Y. W. Mu, G. M. Ren, H. J. Zhai and S. D. Li, *Phys. Chem. Chem. Phys.*, 2016, **18**, 11610.
15 Q. Chen, H. R. Li, W. J. Tian, H. G. Lu, H. J. Zhai and S. D. Li, *Phys. Chem. Chem. Phys.*, 2016, **18**, 14186.
16 W. J. Tian, Q. Chen, H. R. Li, M. Yan, Y. W. Mu, H. G. Lu, H. J. Zhai and S. D. Li, *Phys. Chem. Chem. Phys.*, 2016, **18**, 9922.
17 E. Oger, N. R. M. Crawford, R. Kelting, P. Weis, M. M. Kappes and R. Ahlrichs, *Angew. Chem. Int. Ed.*, 2007, **46**, 8503.
18 C. Romanescu, T. R. Galeev, W. L. Li, A. I. Boldyrev and L. S. Wang, *Acc. Chem. Res.*, 2013, **46**, 350.
19 I. A. Popov, T. Jian, G. V. Lopez, A. I. Boldyrev and L. S. Wang, *Nat. Commun.*, 2015, **6**, 8654.
20 T. Jian, W. L. Li, X. Chen, T. T. Chen, G. V. Lopez, J. Li and L. S. Wang, *Chem. Sci.*, 2016, **7**, 7020.
21 W. L. Li, T. Jian, X. Chen, H. R. Li, T. T. Chen, X. M. Luo, S. D. Li, J. Li and L. S. Wang, *Chem. Commun.*, 2017, **53**, 1587.
22 S. R. Daly, P. M. B. Piccoli, A. J. Schultz, T. K. Todorova, L. Gagliardi and G. S. Girolami, *Angew. Chem., Int. Ed. Engl.*, 2010, **49**, 3379.
23 A. Hermann, M. Lein and P. Schwerdtfeger, *Angew. Chem., Int. Ed. Engl.*, 2007, **46**, 2444.
24 Y. Komura and K. Tokunaga, *Acta Crystallogr., Sect. B: Struct. Crystallogr. Cryst. Chem.*, 1980, **36**, 1548.
25 H. W. Sheng, W. K. Luo, F. M. Alamgir, J. M. Bai and E. Ma, *Nature*, 2006, **439**, 419.
26 H. R. Li, H. Liu, X. X. Tian, W. Y. Zan, Y. W. Mu, H. G. Lu, J. Li, Y. K. Wang and S. D. Li, *Phys. Chem. Chem. Phys.*, 2017, **19**, 27025.
27 H. Bai, Q. Chen, H. J. Zhai and S. D. Li, *Angew. Chem., Int. Ed.*, 2014, **54**, 941.
28 P. Jin, Q. H. Hou, C. C. Tang and Z. F. Chen, *Theor. Chem. Acc.*, 2015, **134**, 13.
29 L. S. Wang, J. M. Alford, Y. Chai, M. Diener, J. Zhang, S. M. McClure, T. Guo, G. E. Scuseria and R. E. Smalley, *Chem. Phys. Lett.*, 1993, **207**, 354.
30 Y. Chai, T. Guo, C. Jin, R. E. Hautler, L. P. F. Chibante, J. Fure, L. Wang, J. M. Alford and R. E. Smalley, *J. Phys. Chem.*, 1991, **95**, 7564.
31 S. Gunther, *Arch. Math. Phys.*, 1875, **57**, 209.
32 T. Yu, Y. Gao, D. Xu and Z. Wang, *Nano Res.*, 2018, **11**(1), 354.
33 S. Goedecker, *J. Chem. Phys.*, 2004, **120**, 9911.
34 S. Goedecker, W. Hellmann and T. Lenosky, *Phys. Rev. Lett.*, 2005, **95**, 055501.
35 X. Chen, Y. F. Zhao, L. S. Wang and J. Li, *Comput. Theor. Chem.*, 2017, **1107**, 57.
36 D. J. Wales and H. A. Scheraga, *Science*, 1999, **285**, 1368.
37 J. P. Perdew, K. Burke and M. Ernzerhof, *Phys. Rev. Lett.*, 1996, **77**, 3865.
38 J. VandeVondele, M. Krack, F. Mohamed, M. Parrinello, T. Chassaing and J. Hutter, *Comput. Phys. Commun.*, 2005, **167**, 103.
39 C. Adamo and V. Barone, *J. Chem. Phys.*, 1999, **110**, 6158.
40 R. Krishnan, J. S. Binkley, R. Seeger and J. A. Pople, *J. Chem. Phys.*, 1980, **72**, 650.
41 D. Feller, The role of databases in support of computational chemistry calculations, *J. Comput. Chem.*, 1996, **17**, 1571.
42 K. L. Schuchardt, B. T. Didier, T. Elsethagen, L. S. Sun and V. Gurumoorthi, *J. Chem. Inf. Model.*, 2007, **47**, 1045.
43 M. J. Frisch, *et al.*, *Gaussian 09 Revision D.01*, Gaussian Inc., Wallingford CT, 2013.
44 J. Čížek, *Adv. Chem. Phys.*, 1969, **14**, 35.
45 G. D. Purvis and R. J. Bartlett, *J. Chem. Phys.*, 1982, **76**, 1910.
46 K. Raghavachari, G. W. Trucks, J. A. Pople and M. Head-Gordon, *Chem. Phys. Lett.*, 1989, **157**, 479.
47 H. J. Werner, *et al.*, *Molpro, version 2012.1* (http://www.molpro.net).
48 D. Y. Zubarev and A. I. Boldyrev, *Phys. Chem. Chem. Phys.*, 2008, **10**, 5207.
49 E. D. Glendening, J. K. Badenhoop, A. E. Reed, J. E. Carpenter, J. A. Bohmann, C. M. Morales, C. R. Landis and F. Weinhold, *NBO 6.0*, 2013 (http://nbo6.chem.wisc.edu).
50 H. Prinzbach, A. Weiler, P. Landenberger, F. Wahl, J. Worth, L. T. Scott, M. Gelmont, D. Olevano and B. V. Issendorff, *Nature*, 2000, **407**, 60.
51 J. Lv, Y. C. Wang, L. J. Zhang, H. Q. Lin, J. J. Zhao and Y. M. Ma, *Nanoscale*, 2015, **7**, 10482.
52 G. J. Wang, M. F. Zhou, J. T. Gorttel, G. J. Schrobilgen, J. Su, J. Li, T. Schloder and S. Riedel, *Nature*, 2014, **514**, 475.
53 D. Ciuparu, R. F. Klie, Y. M. Zhu and L. Pfefferle, *J. Phys. Chem. B*, 2004, **108**, 3967.

